Adiabatic reduction and hysteresis of the LFI-model for NO+NH_3 on Pt{100}.

H.Uecker[1], R. Imbihl[2].

[1)]Mathematisches Institut I, Universität Karlsruhe, Germany.

[2)]Institut für Physikalische Chemie und Elektrochemie. Universität Hannover. Hannover. Germany.

M. Rafti, I.M.Irurzun[a),(*)], J.L. Vicente , E.E. Mola.

Instituto de Investigaciones Fisicoquímicas Teóricas y Aplicadas (INIFTA), Universidad Nacional de La Plata.

República Argentina.

[a)] Current address: Department of Applied Mathematics and Theoretical Physics. University of Cambridge, UK.

(*) Author to whom correspondence should be addressed.

e-mail: i.m.irurzun@damtp.cam.ac.uk .Fax: +44 1223 765 900

July 30, 2003

Abstract

The Lombardo–Fink–Imbihl (LFI) model for the NO+NH_3 reaction on Pt{100} consists of seven coupled ordinary differential equations (ODE). Here we present a numerical analysis for relaxation oscillations in LFI and show that LFI can not be adiabatically reduced to two coupled ODEs, belonging then to the multicomponent ODEs category. We show that this is because the explicit consideration of the trapping processes of NO from 1×1 to *hex* phases in the kinetic mechanism of the reaction. Our analysis shows that an adiabatic reduction to three coupled ODEs can be achieved. Moreover, we examine in detail the hysteretic behavior.

1 Introduction

The catalytic reduction of NO on metal surfaces has been intensely studied in recent years due to the deleterious effect of NO in the atmosphere[1, 2]. Aside from these practical aspects, work function and mass spectrometric measurements revealed that these reactions very often exhibit interesting dynamical behaviour such as multiple steady states and regular or chaotic temporal oscillations in the rate of the reaction or in the partial pressures of the reactants[3]. These phenomena have been for example observed during the reduction of NO with NH_3 on polycrystalline and single-crystal metal surfaces under ultrahigh vacuum conditions where the reaction proceeds isothermally. Under such conditions the mechanism underlying the oscillatory behavior has been well-established and can be explained by the existence of a reversible adsorbate-induced phase transition in the crystalline structure that causes a periodic switching between two states with different catalytic activity. For example on Pt{100} oscillations are observed associated with a phase transition between *hex* and 1×1 surface structures. The *hex* phase, which is catalytically inactive reverts to the active 1×1–phase due to adsorption of NO upon a critical value of adsorbate coverage[3, 4, 5, 6, 7].

Related with temporal oscillations, the spatiotemporal distribution of adsorbates on the surface has been experimentally investigated by photoemission electron microscopy (PEEM), revealing a rich variety of spatial patterns and waves[3, 4, 5, 6, 7]. These spatial features are well-documented today and are common to a wide class of non-equilibrium systems[8, 9, 10, 11, 12, 13, 14, 15, 16].

From the theoretical point of view kinetic models based upon the phase transition mechanism has been developed to describe temporal behaviour, in the so called mean field approximation[3, 4, 5, 6, 7]. Extensions to describe pattern formation typically introduce diffusion of the mobile species, leading to the reaction-diffusion equation (RDE) formalism, and gas global coupling. While these developments can nicely describe a number of experimentally observed patterns, it is also true that they are usually based on simplistic representations of the real mechanisms governing the chemical reactions. The NO+ NH_3 reaction involves a number of intermediate species whose dynamic must be adequately represented in order to achieve additional insights about the behavior of this system. Also, it has been recently shown that the dynamic behaviour of multicomponent reaction-diffusion systems posses special properties that deserve to be studied[17, 18, 19]. It is desirable then to explore more detailed models of chemical reactions with the final purpose to achieve a realistic representation with

quantitative agreement with experiments.

The aim of the present work is to analyze a detailed kinetic model for NO+NH_3 reaction. We used here the model developed by Imbihl and co-workers[3], (LFI model), which reproduces the overall kinetics as well as the rate oscillations quite well. The LFI model was developed to provide a unified model to both NO+NH_3 and NO+H_2 reactions and is based upon the decisive role of the $1 \times 1 \leftrightarrow hex$ phase-transition. The model considers the evolution of seven different chemical species including adsorption, desorption, dissociation, reaction and trapping processes. Recent experimental measurements of the coverage dependence of sticking probabilities and rate constants were obtained which is not included here[20, 21, 22]. Also it was proposed that the $1 \times 1 \leftrightarrow hex$ phase transition on Pt{100} follows a non-linear power law with the NO coverage in hex phase like in the CO+O_2 reaction[22]. All these features can be introduced in the LFI model but their inclusion implies additional mathematical difficulties which will be the subject of a further work[23]. We used LFI model as a starting point for further investigations.

In the present work we focus ourselves in the analysis of the set of seven coupled ordinary differential equations (ODE's) in the LFI model. We show that the system cannot be adiabatically reduced to a simple two-dimensional ODE system. Due to the mathematical complexity which makes difficult to handle the equations for analytical treatment, we perform the analysis numerically. This shows that a reduction to three coupled ODEs can be achieved. In Section 2, the kinetic model and the numerical method to solve it are presented. In Section 3 we perform a constrained system analysis (CSA) to follows the dynamics of the system. A dynamical adiabatic reduction is performed in Section 4 showing that the system can not be reduced to a two-dimensional ODE system. In Section 3, we study the dependence of the system behavior on temperature. Finally our conclusions are summarized in Section 5.

2 The model

The mechanism of the LFI model can be written as[3]:

$$NO + *_{\mathrm{1x1}} \quad \Leftrightarrow \quad NO_{\mathrm{ad}} \tag{1.1}$$

$$NO + *_{\mathrm{hex}} \quad \Leftrightarrow \quad NO_{\mathrm{ad}} \tag{1.2}$$

$$NH_3 + *_{1x1} \Leftrightarrow NH_{3,1x1} \tag{1.3}$$

$$H_2 + 2*_{1x1} \Leftrightarrow 2H_{1x1} \tag{1.4}$$

$$NO_{\mathrm{ad}} + *_{1x1} \rightarrow N_{1x1} + O_{1x1} \tag{1.5}$$

$$NH_{3,1x1} + 3*_{1x1} \Leftrightarrow N_{1x1} + 3H_{1\times1} \tag{1.6}$$

$$2N_{1x1} \rightarrow N_2 + 2\,*_{1x1} \tag{1.7}$$

$$O_{1x1} + 2H_{1x1} \rightarrow H_2O + 3\,*_{1x1} \tag{1.8}$$

$$1 \times 1 \Leftrightarrow \text{hex} \tag{1.9}$$

$$NO_{\mathrm{hex}} + *_{1\times1} \rightarrow NO_{1\times1} + *_{\mathrm{hex}} \tag{1.10}$$

Here $*_{1\times1}$ denotes a vacant adsorption site on the 1×1 phase, and $*_{\mathrm{hex}}$ a vacant adsorption site on the hex phase. Steps (1.1)-(1.4) represent NO, NH_3 , and H_2 adsorption and desorption. Step (1.5) corresponds to the dissociation of NO, which on Pt{100} occurs above T$\approx$ 380K. In (1.8) is assumed that the reaction product H_2O desorbs immediately after formation, while atomic nitrogen which may desorb as N_2 via reaction (1.7) has a finite residence time on the surface. As an alternative reaction channel, N_{ad} may also recombine with H_{ad} to form NH_3 as denoted by step (1.6). We refer to the reader to Ref [3] and references therein for a detailed description of the mechanism.

This mechanism yields to a set of seven ODEs:

$$\frac{d}{dt}\theta_{NO}^{1\times1} = F_{NO}p_{NO}(\theta_{1\times1} - \theta_{NO}^{1\times1} - 4\theta_{NH_3}^{1\times1}) - k_1\theta_{NO}^{1\times1} - k_2\frac{\theta_{NO}^{1\times1}\theta_{empty}^{1\times1}}{\theta_{1\times1}} + k_3\theta_{NO}^{hex}\theta_{1\times1} \tag{2.1}$$

$$\frac{d}{dt}\theta_{NO}^{hex} = F_{NO}p_{NO}(\theta_{hex} - \theta_{NO}^{hex}) - k_3\theta_{NO}^{hex}\theta_{1\times1} - k_4\theta_{NO}^{hex} \tag{2.2}$$

$$\frac{d}{dt}\theta_{1\times1} = \left\{ \begin{array}{l} (\frac{d}{dt}\theta_{NO}^{1\times1})/\theta_{grow}^{1\times1} \text{ if } \frac{d}{dt}\theta_{NO}^{1\times1} > 0 \text{ and } \theta_{NO}^{1\times1} \geq \theta_{grow}^{1\times1}\theta_{1\times1} \text{ and } \theta_{1\times1} < 1 \\ -k_{11}(\theta_{1\times1} - \theta_{def}^{hex})(1-c) \text{ if } \theta_{1\times1} > \theta_{def}^{hex} \text{ and } c < 1 \\ 0 \text{ otherwise} \end{array} \right\} \tag{2.3}$$

$$\frac{d}{dt}\theta_{NH_3}^{1\times1} = F_{NH_3}p_{NH_3}(\theta_{1\times1} - 3\theta_{NH_3}^{1\times1} - 1.6\theta_{NO}^{1\times1}) - k_5\theta_{NH_3}^{1\times1} - k_6\frac{\theta_{NH_3}^{1\times1}[\theta_{1\times1} - \theta_H^{1\times1} - 2.5(\theta_O^{1\times1} + \theta_N^{1\times1})]}{\theta_{1\times1}} + k_7\frac{\theta_N^{1\times1}\theta_H^{1\times1}}{\theta_{1\times1}} \tag{2.4}$$

$$\frac{d}{dt}\theta_O^{1\times1} = k_2\frac{\theta_{NO}^{1\times1}\theta_{empty}^{1\times1}}{\theta_{1\times1}} - k_8\frac{\theta_O^{1\times1}\theta_N^{1\times1}}{\theta_{1\times1}} \tag{2.5}$$

$$\frac{d}{dt}\theta_N^{1\times1} = k_2\frac{\theta_{NO}^{1\times1}\theta_{empty}^{1\times1}}{\theta_{1\times1}} + k_6\frac{\theta_{NH_3}^{1\times1}[\theta_{1\times1} - \theta_H^{1\times1} - 2.5(\theta_O^{1\times1} + \theta_N^{1\times1})]}{\theta_{1\times1}} \tag{2.6}$$

$$
\begin{aligned}
& -k_7\frac{\theta_N^{1\times1}\theta_H^{1\times1}}{\theta_{1\times1}} - k_9\frac{(\theta_N^{1\times1})^2}{\theta_{1\times1}} \\
\frac{d}{dt}\theta_H^{1\times1} &= F_{H_2}p_{H_2}\frac{[\theta_{1\times1}-\theta_H^{1\times1}-2.5(\theta_O^{1\times1}+\theta_N^{1\times1})]^2}{\theta_{1\times1}} \\
& +3k_6\frac{\theta_{NH_3}^{1\times1}[\theta_{1\times1}-\theta_H^{1\times1}-2.5(\theta_O^{1\times1}+\theta_N^{1\times1})]}{\theta_{1\times1}} \\
& -3k_7\frac{\theta_N^{1\times1}\theta_H^{1\times1}}{\theta_{1\times1}} - 2k_8\frac{\theta_O^{1\times1}\theta_N^{1\times1}}{\theta_{1\times1}} - k_{10}\frac{(\theta_H^{1\times1})^2}{\theta_{1\times1}}
\end{aligned} \tag{2.7}
$$

where the coverages of the adsorbed species are normalised by the total number of sites. The temperature dependence of the rate constants $k_1,\ldots,k_{11}$ is expressed via the Arrhenius–law $k_i = \nu_i e^{-E_i/RT}$, see Table 1. The coverage dependence of NO and NH_3 desorption is taken into account by

$$
E_1 = E_1^0 - \alpha(\theta_{\rm NO}^{1\times1}/\theta_{1\times1})^2, \quad E_5 = E_5^0 - \phi(\theta_{\rm NH_3}^{1\times1}/\theta_{1\times1})^2 \tag{3}
$$

The inhibitory effect of adsorbates on NO dissociation and the stabilizing effect of adsorbates for the 1×1 phase in Eqs (2) are given by

$$
\theta_{\rm empty}^{1\times1} = \max[(\theta_{1\times1}-\frac{\theta_{\rm NO}^{1\times1}}{\theta_{\rm NO}^{\rm inh}}-\frac{\theta_{\rm O}^{1\times1}}{\theta_{\rm O}^{\rm inh}}),0] + \max[(\theta_{\rm def}^{1\times1}-\theta_{\rm O}^{1\times1}),0] \tag{4}
$$

$$
c = (\frac{\theta_{\rm NO}^{1\times1}}{\theta_{\rm NO}^{\rm crit}}+\frac{\theta_{\rm O}^{1\times1}}{\theta_{\rm O}^{\rm crit}})/\theta_{1\times1}, \theta_{1\times1}+\theta_{\rm hex}=1, \theta_{\rm def}^{1\times1}=\theta_{1\times1}\theta_{\rm def}, \theta_{\rm def}^{\rm hex}=\theta_{\rm hex}\theta_{\rm def}. \tag{5}
$$

and the further parameters are given in Table 2. A single adsorption site was assumed for all adsorbates so that $\theta_{\rm NO}^{1\times1}+\theta_{\rm NH_3}^{1\times1}+\theta_{\rm O}^{1\times1}+\theta_{\rm N}^{1\times1}+\theta_{\rm H}^{1\times1}\le\theta_{1\times1}$. A certain number of static defect sites, given by θ_{def}, were distributed homogeneously over the surface assuming that NO dissociation can occur more easily there. The condition $\theta_{1\times1}<1$ in the first line of the right hand side of Eq. (2.3) was not explicitly displayed in Ref[3] ; it takes effect at the lower temperature threshold $T\approx 404$K for kinetic oscillations and ensures $\theta_{1\times1}\le 1$. In Eq. (2.3) $\theta_{grow}^{1\times1}$ is the coverage of NO on 1×1 phase for which the growth of islands occurs. Further details of these ODEs are given in Ref[3]. All our calculations, concerning with the $NO+NH_3$ reaction, were made at $p_{NO}=1.1\times10^{-6}$mbar and $p_{NH_3}=4.7\times10^{-6}$mbar.

The system of Eqs (2) is very stiff and the oscillations are of relaxation type involving widely different time scales. An appropriate ODE numerical solver is the linearly implicit extrapolation solver `limex`[24]. Moreover, `limex` can also be used to integrate differential algebraic equations (DAE)

$$
B(X)\frac{\rm d}{{\rm d}t}X = f(X), \quad X\in\Omega\subset R^d, \quad B(X)\in R^{d\times d} \tag{6}
$$

where $B(X)$ may be singular. For general equations

$$\frac{\mathrm{d}}{\mathrm{d}t}X = f(X) \tag{7}$$

this allows a very easy test whether components of X have no own dynamics and can be eliminated adiabatically. Clearly, Eq. (7) is of the form of Eq.(6) with $B = \mathrm{diag}(b_1, \ldots, b_d) = \mathrm{diag}(1, \ldots, 1)$. Hence, we may test for slaved X_i, $i \in I$, where $I \subset \{1, \ldots, d\}$ is some index–set, by simply setting $b_i = 0, i \in I$ and integrating Eq(6). If this yields (approximately, in some part of Ω) the same results as integration of Eq(7) then components X_i, $i \in I$, are slaved (in that part of Ω). In chemical kinetics setting the time derivatives of some reaction intermediates equal to zero is known as quasi steady state approximation.

3 Constrained System Analysis (CSA)

A method[25] which yields insights into the mechanism of kinetic oscillations is what here we call constrained system analysis (CSA). In the CSA, the coverages and the reaction rates are calculated as functions of $\theta_{1\times1}$ by setting $\frac{\mathrm{d}}{\mathrm{d}t}\theta_{1\times1} = 0$ in Eq. (2.3) and letting this so-called constrained system converge to a stable fixed point. To understand the effect of CSA on the dynamics of the system we use the phase picture of oscillatory systems. The evolution of systems describing temporal oscillations can be represented in the phase space, in which time is considered as an implicit variable. In this phase space the system moves on a limit cycle which depends on temperature and that we call periodic orbit $\gamma(T)$. In general then, we use this name to indicate the temporal evolution of the entire set of variables, during an oscillatory period. A periodic orbit $\gamma(425)$ of the system of Eqs.(2) at $T = 425$ is shown in Figure 1(a), together with the temporal evolution of the production rates $\mathrm{r}_{\mathrm{N_2}}$ of N_2 and $\mathrm{r}_{\mathrm{H_2O}}$ of H_2O. The relaxation type oscillations are cut into four segments. The decay of $\theta_{1\times1}$ sets the slowest time scale in the largest segment which is segment 1. Here all other variables follow $\theta_{1\times1}$ adiabatically. This breaks down in segments 2 and 3, where NO adsorption lifts the hex reconstruction. In segment 4 the so-called "surface explosion" occurs with rapid increase in the production of N_2 and H_2O. The explosive behavior is due to the autocatalytic increase in the number of vacant sites. These sites are required for the rate-limiting step of NO dissociation to take place. NH_3 adsorption leads to the build up of an $\mathrm{NH_{x,ad}/H_{ad}}$ layer. This layer is unable to stabilize the 1×1 phase, which leads to the slow

relaxation to the hex phase in segment 1.

In Figure 1(b) we compare the phase plane portraits of the orbit from Fig 1(a) (dots) with the results of a CSA (lines). The plots of the CSA were obtained by increasing $\theta_{1\times1}$ coverage value in steps of 0.01 units from 0.125 to 0.75 and then decreasing it again down to 0.125. These two numbers are the minimum and maximum coverage values for which the CSA converges to a fixed point. Within this range of $\theta_{1\times1}$, the constrained system shows bistability for $0.125 \leq \theta_{1\times1} \leq 0.6$, because two fixed-points co-exist for each value of $\theta_{1\times1}$, yielding two branches in Fig 1(b) (except for $\theta_{\rm NO}^{1\times1}$ as we explain below). The branch associated with a high (low) reaction rate (the full–line (dotted) branch), is called the lower (upper) branch. Outside this range the system is monostable.

The fact that in Fig.1 (b) there is only one branch for $\theta_{\rm NO}^{\rm hex}$ follows from Eq. (2.2). This equation is linear in $\theta_{\rm NO}^{\rm hex}$ and otherwise only contains $\theta_{1\times1}$; hence it can have only one fixed point for each fixed value of $\theta_{1\times1}$.

The constrained system can now be compared to the solution of the full system of Eqs (2). The density of points in the plots of $\gamma(425)$ shows how fast a certain branch is transversed. There is excellent agreement of the slow segment 1 of $\gamma(425)$ with the upper branch from the CSA. However, $\theta_{1\times1}$ stays essentially constant in time in segments 2 and 4(see Fig 1(a)) and hence, these segments can not be captured by CSA. Segments 2 and 4 represent in phase portraits fast transitions between the branches. In segment 3 a considerable error is seen between $\gamma(425)$ and CSA. The CSA is an approximate method that only gives information in those regions in which the variables can follow $\theta_{1\times1}$ adiabatically. However, it must fail in segments 2 and 4 where fast transitions between two branches occur associated with the chemically very important surface explosion. We believe that similar care must be taken in the application of CSA to related systems[25].

4 Adiabatic reduction

First we introduce some notation. We set $X = (y, z)$ with $y = (\theta_{\rm NO}^{1\times1}, \theta_{\rm NO}^{\rm hex}, \theta_{1\times1})$ and $z = (\theta_{\rm NH_3}^{1\times1}, \theta_{\rm O}^{1\times1}, \theta_{\rm N}^{1\times1}, \theta_{\rm H}^{1\times1})$, and write Eqs.(2) in the form:

$$\frac{\rm d}{{\rm d}t}\begin{pmatrix} y \\ z \end{pmatrix} = \begin{pmatrix} f^y((y,z);T,p) \\ f^z((y,z);T,p) \end{pmatrix} \tag{8}$$

where $f^y : R^7 \to R^3$ and $f^z : R^7 \to R^4$ denote the respective right hand sides in Eqs (2) and $p \in R^{11}$ denotes the vector of temperature–independent parameters from Table 2, while T denotes the temperature. Figures 2 (a) and (b) illustrate that (on the periodic orbit γ) z can be eliminated from Eqs (2) adiabatically. Here, for initial conditions on the periodic orbit, using `limex` we integrate Eqs (2) in the form of Eq. (6) with $B(X) = \mathrm{diag}(1,1,1,0,0,0,0)$, i.e., we integrate the DAE

$$\frac{\mathrm{d}}{\mathrm{d}t} y = f^y(y,z), \quad 0 = f^z(y,z) \tag{9}$$

In the following we call this method *implicit reduction*. In Figure 2(a) we compare time–series for some components and the reaction rates of the solution of implicit reduction (dotted lines) with the original periodic orbit $\gamma(425)$ for Eqs(2), i.e. Eq. (8), (full lines). Obviously, the agreement is very good, except for a slightly smaller period for the solution of Eq.(9).

In the orbital plots in Figure 2(b) we compare the two solutions (solution of implicit reduction using +) for three projections in phase space, which cover the seven components of X and the two reaction rates.

We conclude that the system can *in principle* be reduced to the three dimensional ODE

$$\frac{\mathrm{d}}{\mathrm{d}t} y = f^y(y, h(y)) =: g(y), \quad \text{where } z = h(y) \text{ solves } f^z(y,z) = 0 \tag{10}$$

i.e., to an ODE for the slow components $y = (\theta^{1\times1}_{\mathrm{NO}}, \theta^{\mathrm{hex}}_{\mathrm{NO}}, \theta_{1\times1})$ alone. However, two questions immediately arises: 1) can we solve (explicitly) the (nonlinear, coupled) algebraic system $0 = f^z(y,z)$ for $z = z(y)$? 2) can we walk off the periodic orbit obtained with the implicit reduction method and does it drive us back to the periodic orbit?, i.e. does the reduction work in a sufficiently large neighborhood of the periodic orbit?

Explicitly, the system $0 = f^z(y,z)$ reads

$$\begin{aligned}
0 &= F_{NH_3} p_{NH_3} (\theta_{1\times1} - 3\theta^{1\times1}_{NH_3} - 1.6\theta^{1\times1}_{NO}) - k_5 \theta^{1\times1}_{NH_3} \\
&\quad - k_6 \frac{\theta^{1\times1}_{NH_3}[\theta_{1\times1} - \theta^{1\times1}_H - 2.5(\theta^{1\times1}_O + \theta^{1\times1}_N)]}{\theta_{1\times1}} + k_7 \frac{\theta^{1\times1}_N \theta^{1\times1}_H}{\theta_{1\times1}} \qquad (11.1) \\
0 &= k_2 \theta^{1\times1}_{NO} \theta^{1\times1}_{empty} - k_8 \theta^{1\times1}_O \theta^{1\times1}_N \qquad (11.2) \\
0 &= k_2 \theta^{1\times1}_{NO} \theta^{1\times1}_{empty} + k_6 \theta^{1\times1}_{NH_3}[\theta_{1\times1} - \theta^{1\times1}_H - 2.5(\theta^{1\times1}_O + \theta^{1\times1}_N)] \qquad (11.3) \\
&\quad - k_7 \theta^{1\times1}_N \theta^{1\times1}_H - k_9 (\theta^{1\times1}_N)^2
\end{aligned}$$

$$
\begin{aligned}
0 &= F_{H_2} p_{H_2} [\theta_{1\times1} - \theta_H^{1\times1} - 2.5(\theta_O^{1\times1} + \theta_N^{1\times1})]^2 \\
&\quad + 3k_6 \theta_{NH_3}^{1\times1} [\theta_{1\times1} - \theta_H^{1\times1} - 2.5(\theta_O^{1\times1} + \theta_N^{1\times1})] \\
&\quad - 3k_7 \theta_N^{1\times1} \theta_H^{1\times1} - 2k_8 \theta_O^{1\times1} \theta_H^{1\times1} - k_{10} (\theta_H^{1\times1})^2
\end{aligned} \tag{11.4}
$$

and we need to solve for $\theta_{\mathrm{NH_3}}^{1\times1}, \theta_{\mathrm{O}}^{1\times1}, \theta_{\mathrm{N}}^{1\times1}, \theta_{\mathrm{H}}^{1\times1}$ as functions of $\theta_{\mathrm{NO}}^{1\times1}$, $\theta_{\mathrm{NO}}^{\mathrm{hex}}$ and $\theta_{1\times1}$. Clearly, we cannot expect a simple solution for this (highly) nonlinear coupled system. However, we can use some ad hoc simplifications and check a posteriori if the reduction works. We ignore the nonlinear correction to E_5 in Eq.(3) and write down the solution of Eqs.(12) as if the system was uncoupled. That means we solve Eq. (11.1) for $\theta_{\mathrm{NH_3}}^{1\times1}$ while fixing the remaining variables, Eq (11.2) for $\theta_{\mathrm{O}}^{1\times1}$ and so on. This yields:

$$
\theta_{NH_3}^{1\times1} = \frac{F_{NH_3} p_{NH_3} (\theta_{1\times1} - 1.6\theta_{NO}^{1\times1}) + (k_7 \theta_N^{1\times1} \theta_H^{1\times1})/\theta_{1\times1}}{3F_{NH_3} p_{NH_3} + k_5 + k_6 [\theta_{1\times1} - \theta_H^{1\times1} - 2.5(\theta_O^{1\times1} + \theta_N^{1\times1})]/\theta_{1\times1}} \tag{12.1}
$$

$$
\theta_O^{1\times1} = \left\{ \begin{array}{ll}
0 & \mathrm{case}(00) \\
k_2 \theta_{NO}^{1\times1} (\theta_{1\times1} - \theta_{NO}^{1\times1}/\theta_{NO}^{inh})/(k_2 \theta_{NO}^{1\times1}/\theta_O^{inh} + k_8 \theta_H^{1\times1}) & \mathrm{case}(10) \\
k_2 \theta_{NO}^{1\times1} \theta_{def}^{1\times1}/(k_2 \theta_{NO}^{1\times1} + k_8 \theta_H^{1\times1}) & \mathrm{case}(01) \\
k_2 \theta_{NO}^{1\times1} (\theta_{1\times1}(1 + \theta_{def}^{1\times1}) & \\
\quad - \theta_{NO}^{1\times1}/\theta_{NO}^{inh})/(k_2 \theta_{NO}^{1\times1}(1 + 1/\theta_O^{inh}) + k_8 \theta_H^{1\times1}) & \mathrm{case}(11)
\end{array} \right\} \tag{12.2}
$$

$$
\theta_N^{1\times1} = -\alpha_1/2 + \sqrt{\alpha_1^2/4 - \beta_1} \tag{12.3}
$$

$$
\begin{aligned}
\alpha_1 &= (k_7 \theta_H^{1\times1} + 2.5 k_6 \theta_{NH_3}^{1\times1} \theta_O^{1\times1})/k_9 \\
\beta_1 &= k_6 \theta_{NH_3}^{1\times1} (\theta_H^{1\times1} + 2.5\theta_O^{1\times1} - \theta_{1\times1} - 2k_2 \theta_{empty}^{1\times1})/k_9
\end{aligned}
$$

$$
\theta_H^{1\times1} = -\alpha_2/2 + \sqrt{\alpha_2^2/4 - \beta_2} \tag{12.4}
$$

$$
\begin{aligned}
\alpha_2 &= (2k_8 \theta_O^{1\times1} + 3k_7 \theta_N^{1\times1} + 3k_6 \theta_{NH_3}^{1\times1})/k_{10} \\
\beta_2 &= 3k_6 \theta_{NH_3}^{1\times1} (2.5(\theta_O^{1\times1} + \theta_N^{1\times1}) - \theta_{1\times1})/k_{10}.
\end{aligned}
$$

In (12.2), the binary notation 'case(ab)' refers to the two max in the function:

$$
\theta_{\mathrm{empty}}^{1\times1} = \max[(\theta_{1\times1} - \frac{\theta_{\mathrm{NO}}^{1\times1}}{\theta_{\mathrm{NO}}^{\mathrm{inh}}} - \frac{\theta_{\mathrm{O}}^{1\times1}}{\theta_{\mathrm{O}}^{\mathrm{inh}}}), 0] + \max[(\theta_{\mathrm{def}}^{1\times1} - \theta_{\mathrm{O}}^{1\times1}), 0] \tag{13}
$$

with $a = 1$ ($b = 1$) denoting the case that the first (the second) max is greater 0. In (11.3) and (11.4) we take the positive root for physical reasons.

The next step would be to simplify, e.g., (12.1) to

$$\theta^{1\times1}_{\mathrm{NH_3}} = \frac{\mathrm{F_{NH_3}p_{NH_3}}}{3\mathrm{F_{NH_3}p_{NH_3}} + \mathrm{k_5} + \mathrm{k_6}}(\theta_{1\times1} - 1.6\theta^{1\times1}_{\mathrm{NO}}) \tag{14}$$

where we used that $\theta^{1\times1}_{\mathrm{H}} - 2.5(\theta^{1\times1}_{\mathrm{O}} + \theta^{1\times1}_{\mathrm{N}})$ is rather small on the periodic orbits. Using the values from Tables 1 and 2 we obtain $\theta^{1\times1}_{\mathrm{NH_3}} \approx \frac{1}{7}(\theta_{1\times1} - 1.6\theta^{1\times1}_{\mathrm{NO}})$ at $T = 425$. Note that $\theta^{1\times1}_{\mathrm{NH_3}}$ in Eq.(14) only depends on $\theta^{1\times1}_{\mathrm{NO}}, \theta_{1\times1}$. Proceeding in this manner we can produce approximate solutions of the coupled system with reasonably simple formulas.

However, here we rather use the Eqs (12) to reduce the system in Eqs(2) *dynamically*, i.e., we solve Eq.(10), keeping the values of $\theta^{1\times1}_{\mathrm{NH_3}}, \theta^{1\times1}_{\mathrm{O}}, \theta^{1\times1}_{\mathrm{N}}, \theta^{1\times1}_{\mathrm{H}}$ as auxiliary variables and in each time–step solve Eqs(11) as an *uncoupled* system. That means, in Eq (12.1) we use $\theta^{1\times1}_{\mathrm{NO}}, \theta^{\mathrm{hex}}_{\mathrm{NO}}, \theta^{1\times1}_{\mathrm{O}}, \theta^{1\times1}_{\mathrm{N}}, \theta^{1\times1}_{\mathrm{H}}$ from the previous time–step to solve for $\theta^{1\times1}_{\mathrm{NH_3}}$, and similarly in Eqs(12.2-4). We call this method *explicit reduction* to distinguished it from the implicit one mentioned above.

Figure 3 (a) compares $\gamma(425)$ with the result of using the explicit reduction method. The initial conditions were chosen on $\gamma(425)$. Clearly, explicit reduction again produces a periodic orbit which we call $\tilde{\gamma}(425)$. There is a slightly bigger error in $\mathrm{r_{H_2O}}$ than in Fig.2(a), but in fact the periods match even better, and a phase shift becomes only visible after several periods.

The points in Figure 3(b) show solutions of explicit reduction for initial conditions off $\tilde{\gamma}(425)$, which we compare again with $\gamma(425)$ (full line). The dotted line represents two periods of $\tilde{\gamma}(425)$. In the $\theta_{1\times1}, \theta^{1\times1}_{\mathrm{NO}}, \theta^{\mathrm{hex}}_{\mathrm{NO}}$ plot on the left the two trajectories are indistinguishable. We see that the explicit reduction works in a neighborhood of $\gamma(425)$, and that after a rather short transient time we go back to $\tilde{\gamma}(425)$. This has been confirmed using several more perturbations of the system off $\gamma(425)$. In the $\theta^{1\times1}_{\mathrm{H}}, \mathrm{r_{N_2}}, \mathrm{r_{H_2O}}$ plot on the right we see that the error for these components is somewhat larger but still acceptable. The behavior of $\theta^{1\times1}_{\mathrm{NH_3}}, \theta^{1\times1}_{\mathrm{O}}, \theta^{1\times1}_{\mathrm{N}}$ is similar to the one in Fig.2(b) middle.

Obviously, the return of the perturbed orbits to $\tilde{\gamma}(425)$ essentially takes place during segment 1 of $\tilde{\gamma}(425)$. This is exactly what we can expect from the CSA in section 3, where we saw the slaving of *all* other variables to $\theta_{1\times1}$. However, the good agreement between $\tilde{\gamma}(425)$ and $\gamma(425)$ also during the "surface explosions" is rather surprising. This again illustrates the fact that the dynamics of the system is constituted by only two processes, the surface phase transition and the so-called "surface explosion". The nucleation of the 1×1 phase on a hex substrate is controlled by the NO coverage on the hex phase. The NO coverage on the 1×1 phase in turn controls the phase transition in the

other direction, i.e. from the 1×1 to the hex phase as well as the ignition of the "surface explosion". The latter happens as the NO coverage falls below a certain limit creating enough vacant sites for NO dissociation to occur and to spread autocatalytically. In conclusion three variables are representing the dynamics of the system $(\theta_{\mathrm{NO}}^{1\times1}, \theta_{\mathrm{NO}}^{\mathrm{hex}}, \theta_{1\times1})$.

Next, we may ask whether we can even reduce Eqs (2) to a two-dimensional ODE by eliminating either $\theta_{\mathrm{NO}}^{1\times1}$ or $\theta_{\mathrm{NO}}^{\mathrm{hex}}$, proceeding as above. This fails because no oscillatory behavior is then found. The NO coverage on the hex phase seems to be an excellent candidate for further elimination because the hex phase is catalytically inactive and the only role of the NO there is to initiate the lifting of the hex reconstruction through NO supply for growing 1×1 islands. This happens in a so-called trapping process in which NO molecules migrate from the hex phase to 1×1 islands and are trapped there because of the higher adsorption energy. Apparently because this is an essential step further elimination is not possible.

5 Temperature dependence and hystereses

One of the strengths of the LFI model is that it not only yields oscillations but also reproduces qualitatively the overall behavior of the reaction system over a wide range of temperatures. Here we show that also our reduction works in this whole T-range. We start with some typical periodic orbits $\gamma(T)$ of Eqs (2) (full lines) and $\tilde{\gamma}(T)$, the orbit of explicit reduction (broken lines) in Figure 4. We restrict to plotting $\theta_{\mathrm{NO}}^{1\times1}, \theta_{\mathrm{NO}}^{\mathrm{hex}}, \theta_{\mathrm{NH_3}}^{1\times1}, \mathrm{r}_{\mathrm{N_2}}$. The initial conditions were deliberately chosen off $\gamma(T)$ (and $\tilde{\gamma}(T)$), in order to illustrate again that the reduction also works off the periodic orbit. The temperatures were chosen near the lower and upper ends of the range of kinetic oscillations. The temperature dependence of the full model of Eqs (2) can be summarized as follows. Kinetic oscillations are observed for $T_0 < T < T_1$, with $T_0 \approx 404\mathrm{K}$, $T_1 \approx 433\mathrm{K}$.

For $T < T_0$, the surface is completely in the 1×1 phase ($\theta_{1\times1} = 1$), while for $T > T_1$ it is in the hex phase ($\theta_{1\times1} = 0$). In both cases, the production rates $\mathrm{r}_{\mathrm{N_2}}$ and $\mathrm{r}_{\mathrm{H_2O}}$ are zero. The periods $\pi(\gamma(T))$ of the oscillations also depend on T, but only slightly except near the boundaries of the existence range.

In Figure 4 we compare $\gamma(T)$ and $\tilde{\gamma}(T)$. Again, the agreement is very good, with a small downshift (upshift) in period for $T = 408\mathrm{K}$ ($T = 433\mathrm{K}$). The error in the components (not shown) is small too. This shows that our explicit reduction also works in these temperature ranges.

In order to study the temperature dependence of the model, we calculate for fixed T averaged quantities like:

$$\langle\theta_{1\times1}\rangle(T) = \frac{1}{\tau}\int_0^\tau \theta_{1\times1}(t)\,\mathrm{d}t \tag{15}$$

for large τ (of the order 10^4sec.). Equivalently, we could average over one period $\pi(T)$ (or $\tilde{\pi}(T)$) but since we want to compare the results of Eqs.(2) and the explicit reduction this would give a slight ambiguity. In Ref [6] , the hysteretic behavior of the reaction rates in NO+NH_3 on Pt100 was not measured under true steady state conditions because the temperature was changed with a heating/cooling rate 0.75K/s. The same problem exist in the numerical simulations of Eqs(2) in Ref [3], where also a temperature ramp was applied. For obtaining the true steady state behavior as a function of temperature we vary the temperature stepwise to $T+\delta$ (with $\delta = \pm 1$K) instead of ramping it.

For the parameters from Tables 1 and 2, the kinetics oscillations are found from 411 K to 433 K in the heating branch (dashed line) and from 433 K to 404 K in the cooling branch (full line). As we show in Figure 5, a hysteresis occurs only in a small T-window at low temperatures. Moreover, Fig.5 shows that the error in the averages between $\gamma(T)$ and $\tilde{\gamma}(T)$ is very small, except for, again, r_{N_2}.

The two branches of the hysteresis differ essentially in the NO coverage on the 1x1 phase. At high NO coverage NO dissociation is inhibited and therefore this branch is catalytically inactive. On the branch with the low NO coverage NO can dissociate freely and therefore this branch is active.

6 Discussion and Conclusions

The primary motivation for this analysis has been that spatially resolved studies of this system showed an interesting sequence of chemical wave patterns transforming finally into a state of chemical turbulence[26, 27]. In order to link these phenomena to local dynamics described by ODE's the complexity of the seven variable system needs first to be reduced before formulating a reaction-diffusion system. CSA has being used in an attempt to identify the slow variables. CSA showed that the time evolution of the variables can be naturally divided in four segments. We can clearly identify the $\theta_{1\times1}$ as a slow variable but this holds only in one of the four segments. Despite a missing clear separation of time scales over the whole oscillation cycle the dynamics of the system can be reproduced quite accurately by only three variables, $(\theta_{\mathrm{NO}}^{1\times1}, \theta_{\mathrm{NO}}^{\mathrm{hex}}, \theta_{1\times1})$ and treating the remaining four variables as "slaved"

by setting their time derivatives equal to zero. The mechanistic basis of this reduction is the decisive role of the surface phase transition and of the "surface explosion" being controlled by the NO coverage on the 1×1 and on the hex phase, respectively. It has been verified that this reduction works through the whole window of oscillatory behaviour (404 K to 434 K), with the agreement between reduced and full system being remarkably good even at the lower and upper temperature limit. It's worth mentioning that we have also neglected the (non-linear) coverage dependence oft he activation energy for ammonia desorption in k_5, in the reduction. Importantly, the system can not be further reduced to a two variables one without loss of oscillatory behavior. This is due to the explicit consideration of the trapping process of NO form 1×1 to hex phases in the kinetic mechanism of the reaction. With the reduced equations as basis the more complex subject of the spatiotemporal dynamics can now be attacked.

7 Acknowledgments

This work was supportted by DAAD (Germany) and Fundación Antorchas (Argentina). E. E. Mola also acknowledge the financial support of Consejo de Investigaciones Científicas y Técnicas (CONICET), Comisión de Investigaciones Científicas de la Provincia de Buenos Aires (CIC) and Universidad Nacional de La Plata (UNLP).

References

[1] W. F. Egelhoff Jr., in *The Chemical Physics of Solid Surfaces and Heterogeneous Catalysis* (D. A. King , D. P. Woodruff editors), Elsevier, Amsterdam, vol. 4 (1982).

[2] M. Shelef. Catal. Rev. Sci. Eng., 11, (1975).

[3] S. J. Lombardo, T. Fink, R. Imbihl, J. Chem. Phys. 98 (1993), 5526.

[4] C. G. Takoudis, L. D. Schmidt, J. Phys. Chem., 87 (1983), 958.

[5] T. Katona, G. A. Somorjai, J. Phys. Chem. 96 (1992), 5465.

[6] S. J. Lombardo, F. Esch, R. Imbihl, Surf. Sci. 271 (1992), L367.

[7] S. J. Lombardo, M. Slinko, T. Fink, T. Löher, H. H. Madden, R. Imbihl, F. Esch, G. Ertl, Surf. Sci. 269/270 (1992) 481.

[8] F. Mertens, G. Veser, A. S. Mikhailov, and R. Imbihl, Synchronization and Breakdown of Global Coupling in Oscillatory Surface Reactions, in Chaos and Complexity, eds. J. Tran Than Van et al. (Editions Frontieres, Gif-sur-Yvette 1995), 285-294.

[9] Reviewed by P. Gray and S. K. Scott, *Chemical Oscillations and Instabilities: Non-Linear Chemical Kinetics*, Oxford University Press,1990.

[10] S. K. Scott, *Chemical Chaos*, Oxford University Press, 1991.

[11] R.Imbihl and G.Ertl, Chem.Rev. 95 (1995) 697.

[12] H. H. Rotermund, in *Pattern Formation in Continuous and Coupled System*, IMA-Series, Springer, New York, 1999, vol. 115, p. 231.

[13] Chaos, Focus Issue: Non linear Pattern Formation in Surface Science, 12 (2002) 107.

[14] E.E. Mola, D.A. King, I. M. Irurzun, J. L. Vicente, Surf. Rev. and Lett. 10 (2003) 23.

[15] I. M. Irurzun, R. B. Hoyle, M. R. E. Proctor, D. A. King, Chemical Physics Letters (2003), in press.

[16] H. Uecker, submitted.

[17] R. Woesler, P. Schutz, M. Bode, M. Or-Guil, H. G. Purwins, Physica D, 91 (1996) 376.

[18] A. M. Zhabotinsky, M. Dolnik, I. R. Epstein, J. Chem. Phys. 103 (1995) 10306.

[19] Or-Guil, M. Bode, C. P. Schenk, H. G. Purwins, Phys. Rev. E 57 (1998) 6432.

[20] J. M. Bradley, A. T. Pasteur, D. A. King, J. Chem. Soc., Faraday Trans., 92 (1996), 2941.

[21] J. M. Bradley, A. Hopkinson, D. A. King, Surface Science, 371 (1997),255.

[22] A . V. Walker, M. Gruyters, D. A. King, Surface Science Letters, 384 (1997). L791.

[23] I. M. Irurzun, private communication.

[24] P. Deuflhard, F. Bornemann. *Scientific computing with ordinary differential equations*, Vol. 42 of *Texts in Applied Mathematics*. Springer-Verlag, New York, 2002 (available on-line at http://www.zib.de/SciSoft/CodeLib/ivpode.en.html).

[25] M. Gruyters, T. Ali, D.A.King, J. Phys. Chem. 100 (1996) 14417.

[26] G. Veser, R. Imbihl, J. Chem. Phys. 96 (1992), 7155.

[27] G. Veser, F. Esch, R. Imbihl, Catal. Lett. 13 (1992) 371.

Figure Captions

Figure 1 :(a) The periodic orbit $\gamma(425)$ for the system of Eqs (2) at $T = 425$K, (b) phase plane portraits of the orbit in (a) (dots) compared to the constrained system analysis (lines). Coverages in ML and the rates in ML/s. The arrows indicate the direction of time

Figure 2 : Comparison of the system of Eqs(2) (full lines) and the implicitly reduced 3d-system (dotted lines) (a) Time series of $\theta_{1\times1}, \theta_{NO}^{1\times1}, \theta_{NO}^{hex}, \theta_{NH_3}^{1\times1}, r_{N_2}, r_{H_2O}$ and , (b) orbital plots. The arrows indicate the direction of time.

Figure 3 : Comparison of the system of Eqs(2) (full lines) and the explicitly reduced 3d-system (dashed lines) (a) Time series of $\theta_{1\times1}, r_{N_2}, r_{H_2O}$ and , (b) orbital plots with initial conditions on the periodic orbit. The points show solution of the explicitly reduced 3d-system for initial condition off the periodic orbit.

Figure 4 : Periodic ODE-orbits $\gamma(T)$ (full line) and $\tilde{\gamma}(T)$(dashed line) at $T = 408$K (a) and $T = 433$ K (b).

Figure 5 : Hysteretic behaviour in the system of Eqs, (2) (lines) when T is varied in a slow cycle. The arrows indicate the change of T. Points indicate the behavior of the explicitly reduced 3d-system. Coverages in ML, reaction rates in ML/s.

Table 1: Rate constants for the NO+NH_3 reaction on Pt{100}[3].

reaction step	parameter	$\nu_i(s^{-1})$	E_i(kcal×mol^{-1})	value at T=425K (s^{-1})
NO-desorption 1×1	k_1	1.7×10^{14}	37.0[a]	1.6×10^{-5}
NO-dissociation 1×1	k_2	2.0×10^{15}	28.5	4.4
NO-trapping on 1×1	k_3	2.2×10^{4}	8.0	1.7
NO-desorption hex	k_4	4.0×10^{12}	26.0	0.17
NH_3-desorption 1×1	k_5	1.0×10^{9}	18.0[a]	0.55
NH_3-dissociation 1×1	k_6	1.0×10^{15}	27.5	7.2
NH_3-formation 1×1	k_7	1.0×10^{10}	16.0	59.1
H_2O-formation 1×1	k_8	1.0×10^{13}	13.0	2.1×10^{6}
N_2-desorption 1×1	k_9	1.3×10^{12}	19.0	2.2×10^{2}
H_2-desorption 1×1	k_{10}	8.0×10^{12}	23.0	11.9
Transition 1×1→hex	k_{11}	2.5×10^{11}	25.0	3.5×10^{-2}

[a]For zero local coverage, see Eq.(3)

Table 2: Temperature independent parameters[3].

description	parameter	value
NO-adsorption flux 1×1, hex	F_{NO}	2.21
NH_3-adsorption flux 1×1	F_{NH_3}	2.84
H_2-adsorption flux 1×1	F_{H_2}	8.28
Parameter for NO desorption activation energy	α	24(kcal×mol^{-1})
Parameter for NH_3 desorption activation energy	ϕ	30(kcal×mol^{-1})
Inhibition coverage of NO for NO-dissociation	θ_{NO}^{inh}	0.61(ML)
Inhibition coverage of O for NO-dissociation	θ_{O}^{inh}	0.399(ML)
Critical coverage of NO for the 1×1→ hex phase transf.	θ_{NO}^{crit}	0.3(ML)
Critical coverage of O for the 1×1→ hex phase transf.	θ_{O}^{crit}	0.4(ML)
Coverage for island growth in the hex→1×1 phase transf.	$\theta_{grow}^{1\times1}$	0.5(ML)
Amount of surface defects	θ_{def}	1.0×10^{-4}(ML)

Figure 1

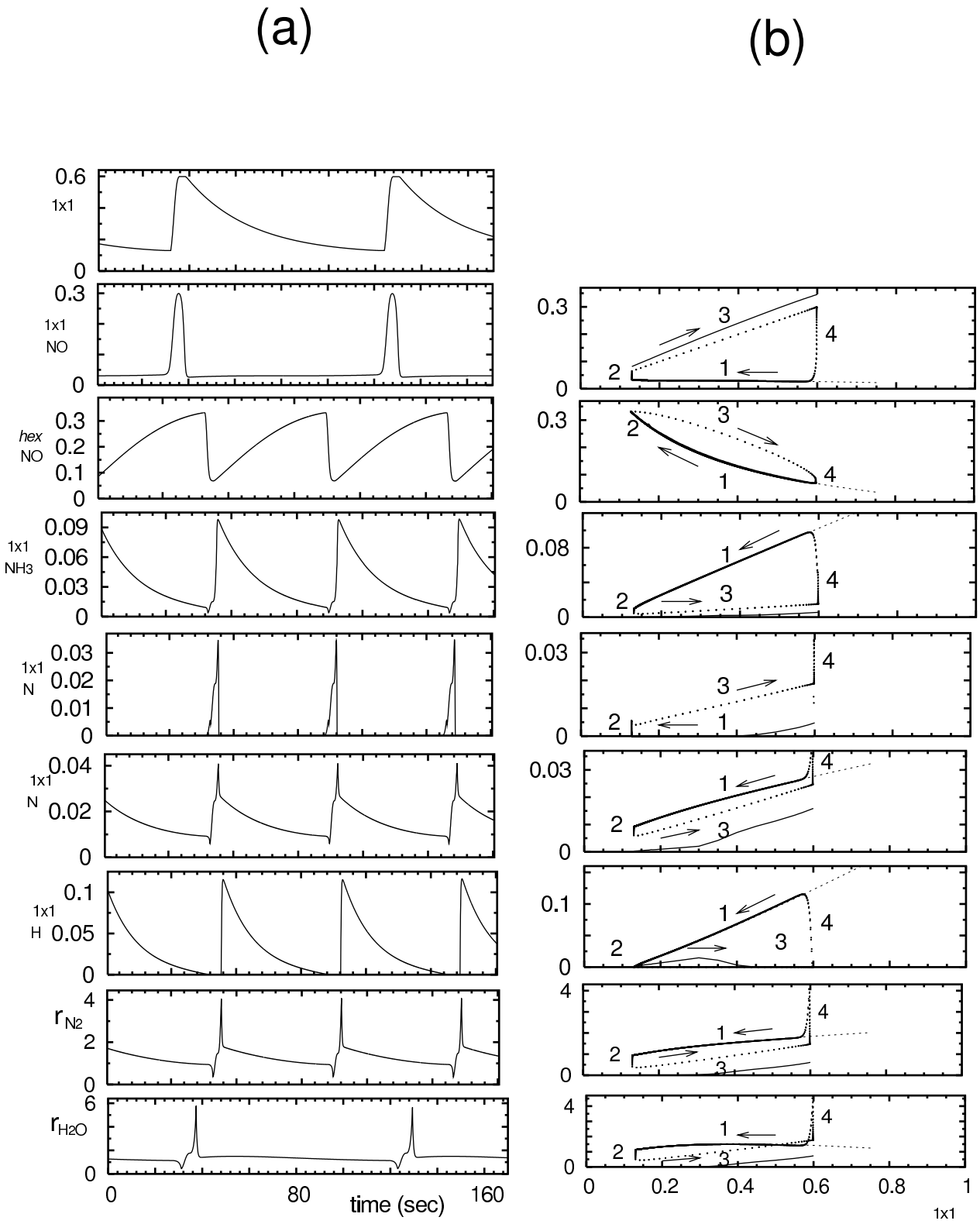
(a)
(b)
0.6
1x1
0
0.3
1x1
NO
0
0.3
0.2
0.1
hex
NO
0
0.09
0.06
0.03
1x1
NH3
0
0.03
0.02
0.01
1x1
N
0
0.04
0.02
1x1
N
0
0.1
0.05
1x1
H
0
4
2
r N2
0
6
r H2O
0
0
80
160
time (sec)
0.3
0
0.3
0
0.08
0
0.03
0
0.03
0
0.1
0
4
0
4
0
0
0.2
0.4
0.6
0.8
1
1x1
1
2
3
4

Figure 3

(a)

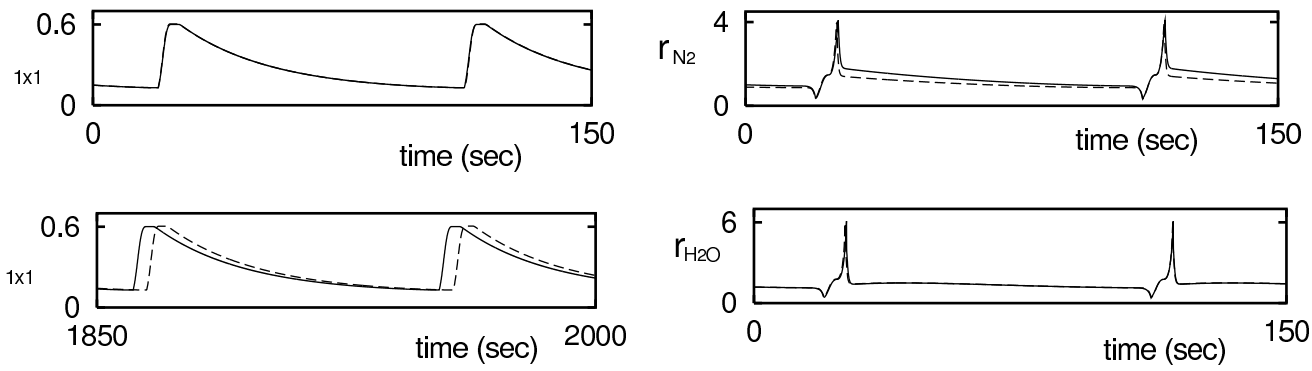
0.6
1x1
0
0
150
time (sec)
r N2
4
0
0
150
time (sec)
0.6
1x1
0
1850
2000
time (sec)
r H2O
6
0
0
150
time (sec)

(b)

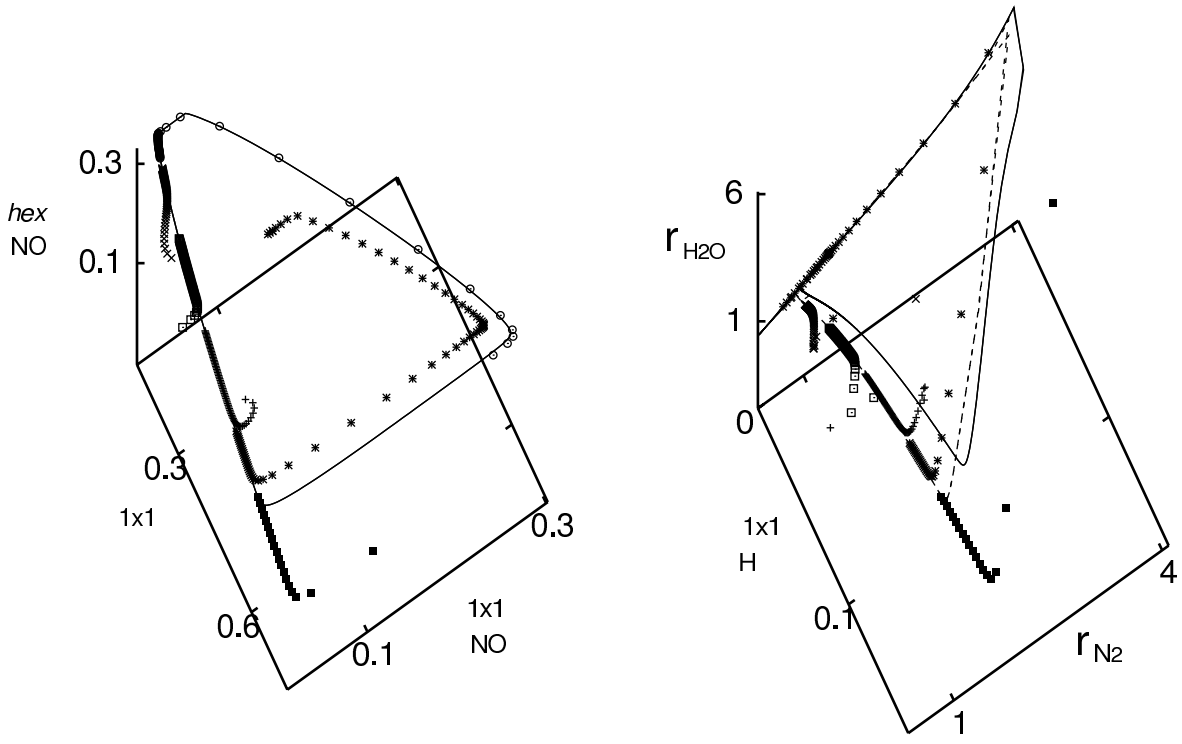
0.3
hex
NO
0.1
0.3
1x1
0.6
0.1
1x1
NO
0.3
r H2O
6
1
0
1x1
H
0.1
1
r N2
4

Figure 5

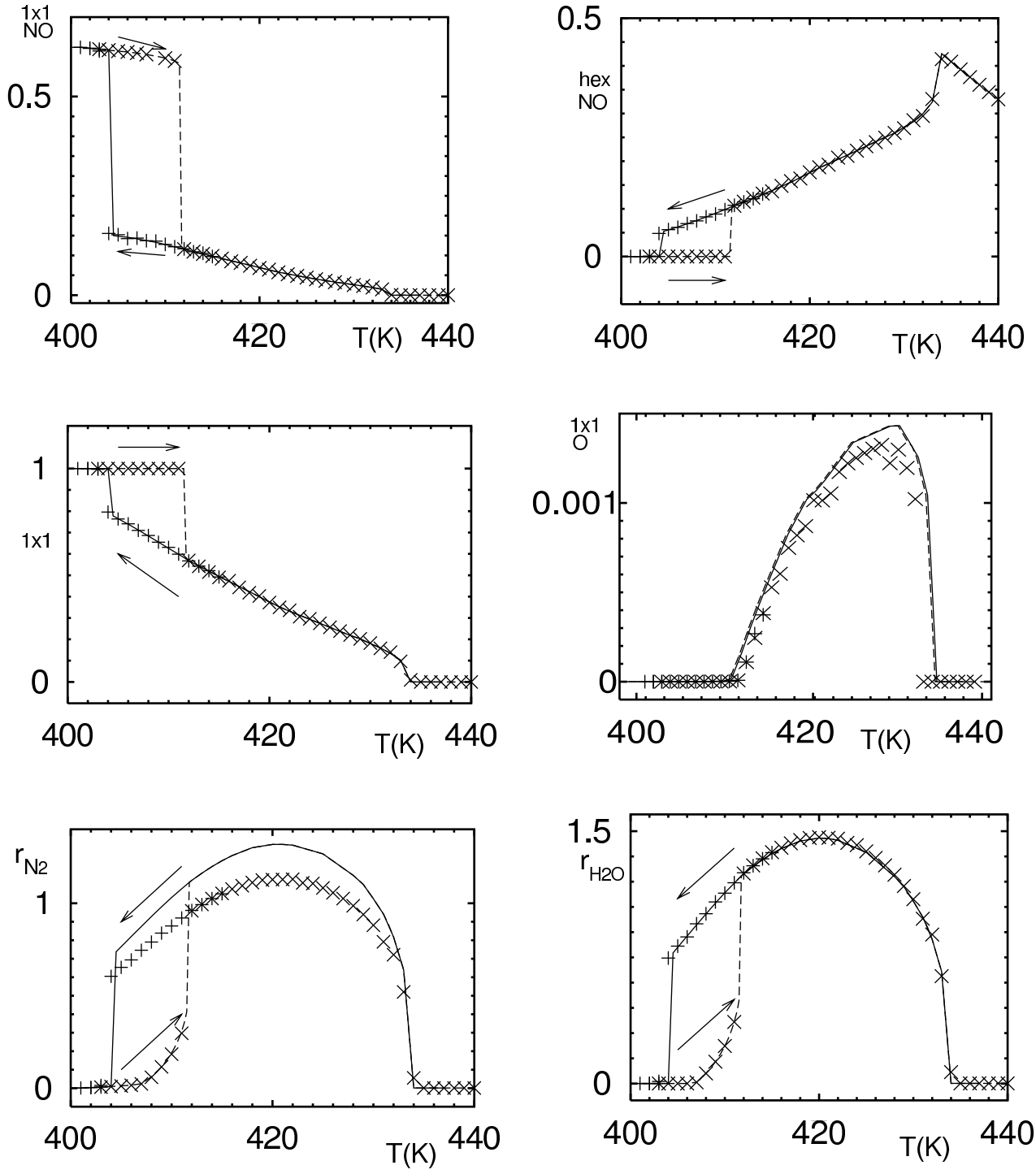
1x1
NO
0.5
0
400
420
T(K)
440
0.5
hex
NO
0
400
420
T(K)
440
1
1x1
0
400
420
T(K)
440
1x1
O
0.001
0
400
420
T(K)
440
r
N2
1
0
400
420
T(K)
440
1.5
r
H2O
0
400
420
T(K)
440

Figure 4

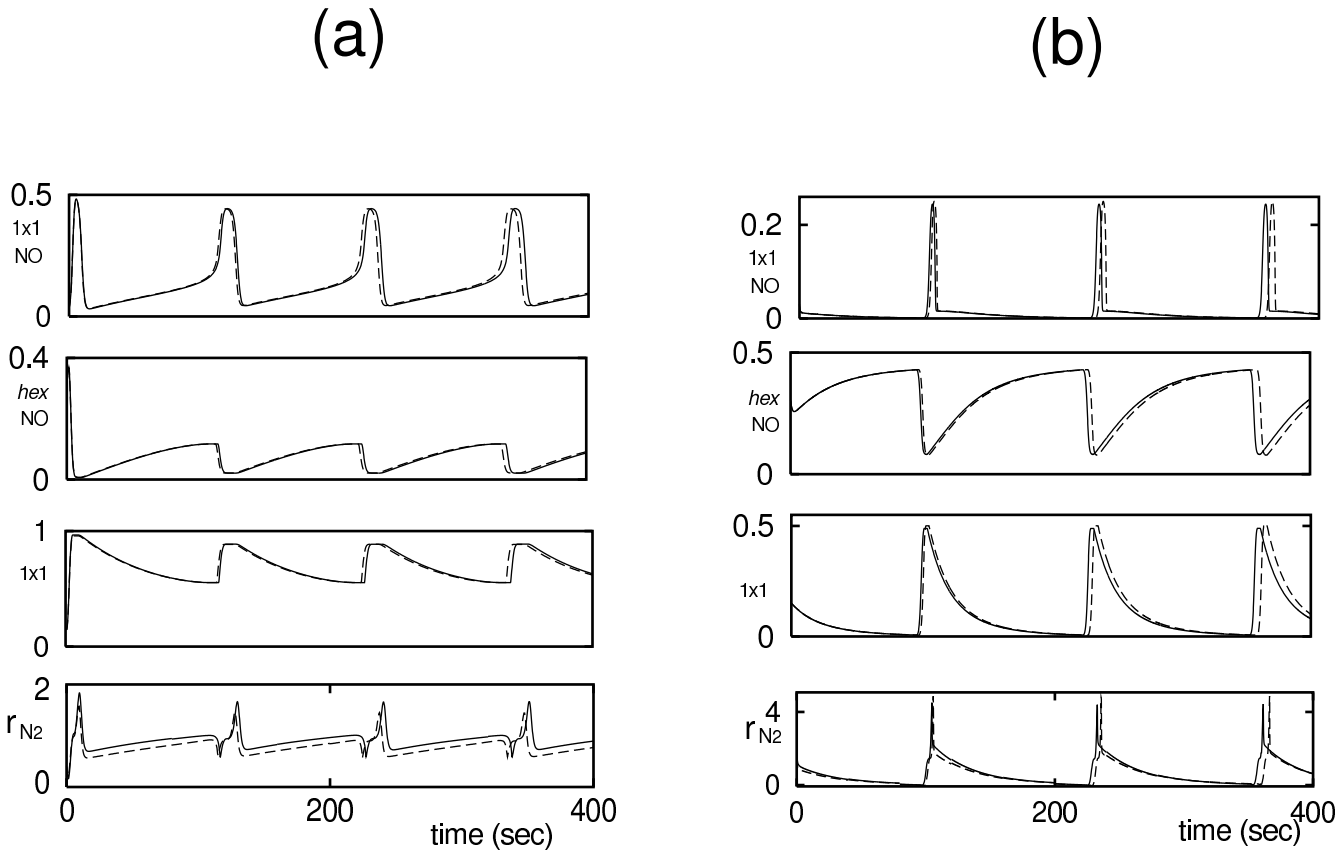
(a)
(b)
0.5
1x1
NO
0
0.4
hex
NO
0
1
1x1
0
2
r N2
0
0
200
400
time (sec)
0.2
1x1
NO
0
0.5
hex
NO
0
0.5
1x1
0
4
r N2
0
0
200
400
time (sec)

Figure 2

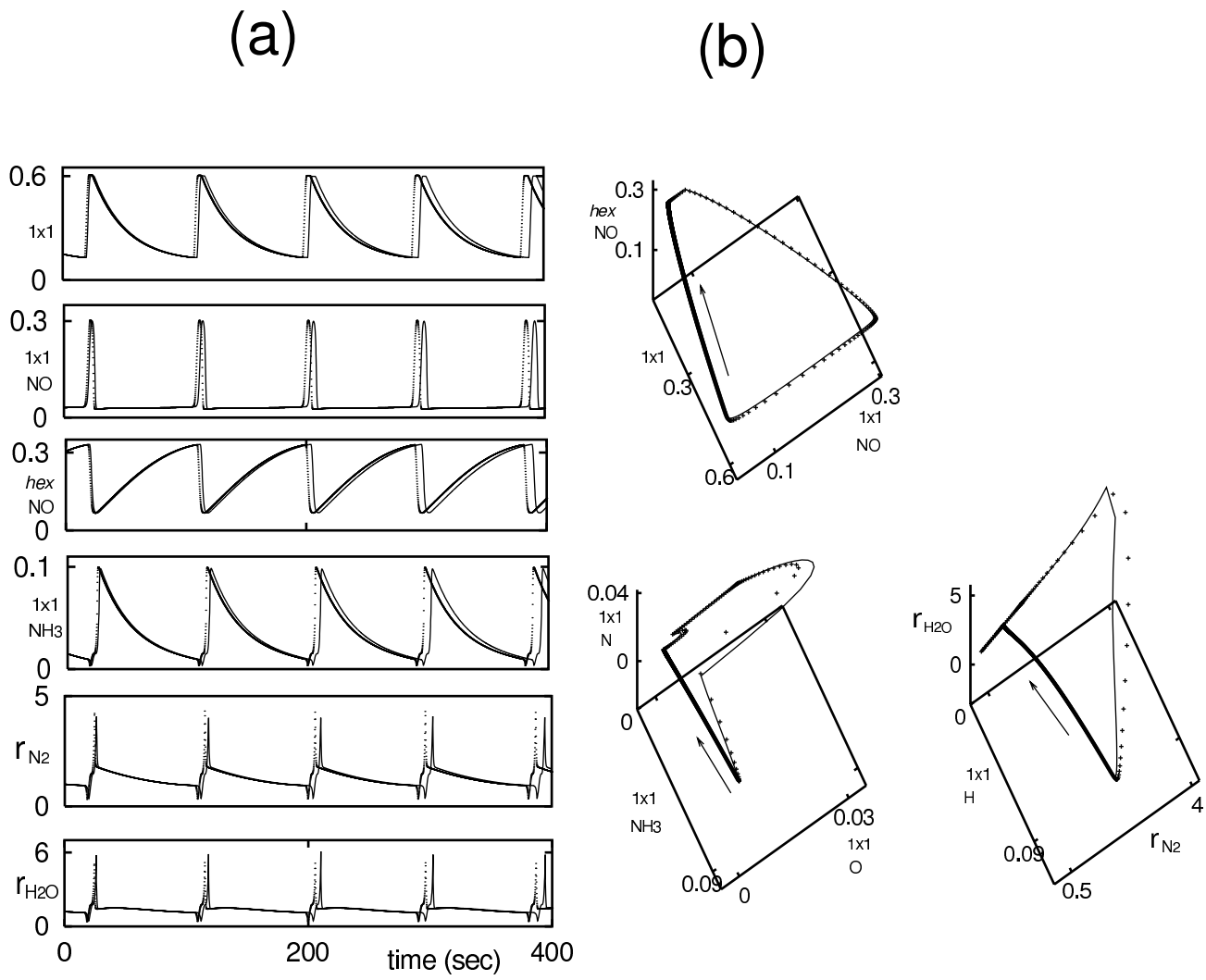
(a)
(b)
0.6
1x1
0
0.3
1x1
NO
0
0.3
hex
NO
0
0.1
1x1
NH3
0
5
r N2
0
6
r H2O
0
0
200
time (sec)
400
0.3
hex
NO
0.1
1x1
0.3
0.6
0.1
0.3
1x1
NO
0.04
1x1
N
0
0
1x1
NH3
0.09
0
0.03
1x1
O
5
r H2O
0
0
1x1
H
0.09
0.5
4
r N2